4

Molten Salt Synthesis of Ceramic Powders

Toshio Kimura
Keio University
Japan

1. Introduction

Molten salt synthesis, one of the methods of preparing ceramic powders, involves the use of a molten salt as the medium for preparing complex oxides from their constituent materials (oxides and carbonates). Ceramic powders are prepared from solid, liquid, and gas phases by various methods (Rahaman, 2003). For large-scale commercial production, ceramic powders are fabricated mainly from the solid phase by a conventional powder metallurgical method. Molten salt synthesis is a modification of the powder metallurgical method. Salt with a low melting point is added to the reactants and heated above the melting point of the salt. The molten salt acts as the solvent.

Molten salts have been used as additives to enhance the rates of solid state reactions for a long time. The amount of salt is small, typically a few percent of the total weight. In contrast, in molten salt synthesis, a large amount of salt is used as the solvent to control powder characteristics (size, shape, etc.). In this sense, molten salt synthesis is different from the flux method, which uses the salt as an additive to enhance the reaction rate.

Typical examples of salts used in molten salt synthesis are chlorides and sulfates. In many cases, eutectic mixtures of salts are used to lower the liquid formation temperature. The melting points of NaCl and KCl are 801°C and 770°C, respectively, and that of 0.5NaCl–0.5KCl (eutectic composition) is 650°C. For example, $0.635Li_2SO_4$–$0.365Na_2SO_4$ is the most commonly used salt among sulfates because of its low melting temperature, which is 594°C, whereas that of Na_2SO_4–K_2SO_4 is 823°C. The solubilities of oxides in molten salts vary greatly from less than 1×10^{-10} mole fraction to more than 0.5 mole fraction, typically 1×10^{-3} - 1×10^{-7} mole fraction (Arendt et al., 1979). In many cases, the formation reaction occurs in the presence of solid reactant particles. In this sense, molten salt is somewhat different from ordinary solvents, which dissolve all reactant particles and the product particles precipitate from a homogeneous liquid phase.

Generally, a complex oxide powder is prepared from reactants by the following procedure. A mixture of the reactants and salt is heated above the melting temperature of the salt. At the heating temperature, the salt melts and the product particles form. The characteristics of the product powder are controlled by selecting the temperature and duration of the heating. Then, the reacted mass is cooled to room temperature and washed with an appropriate solvent (typically, water) to remove the salt. The complex oxide powder is obtained after drying. The procedure is the same as that of a conventional powder metallurgical method and is easily scaled up for the fabrication of large quantities of materials.

The use of molten salt is a common method to grow single crystals from solution (Elwell & Scheel, 1975). In this method, the reactant materials are completely dissolved in molten salt

to obtain a uniform liquid. Upon cooling, solid particles nucleate homogeneously in the liquid phase ("homogeneously" means that a nucleus forms somewhere in the liquid phase). A single crystal with a large size can be obtained by limiting the number of nuclei formed during cooling. Therefore, a salt having a high solubility of the reactant materials is required. Conversely, in molten salt synthesis, a large number of nuclei are necessary to obtain powder particles with an appropriate size, typically from a few tenths to about ten micrometers. The surfaces of the reactant particles are utilized as the nucleation sites. In other words, the product particles nucleate heterogeneously on the surfaces of the reactant particles. Therefore, high solubility for all reactants is not desirable. The control of the cooling rate is very important in the single-crystal growth, because the cooling rate determines the number of nuclei and the size of the product crystals. The cooling rate gives a minor influence on the particle sizes in the molten salt synthesis, because a vast number of particles are already present before cooling and the materials dissolved in the molten salt precipitate on the surfaces of the already existing solid particles.

The role of the molten salts is (1) to increase the reaction rate and lower the reaction temperature; (2) to increase the degree of homogeneity (the distribution of constituent elements in the solid solution); (3) to control particle size; (4) to control particle shape; and (5) to control the agglomeration state. The major purpose of employing molten salt synthesis is (1) to prepare powders for sintering and (2) to prepare anisometric particles. In sintering of powders, a good sintered compact is obtained from a powder with grains of submicrometer size and a low degree of agglomeration (Rahaman, 2003). Recently, textured ceramics are prepared by the templated grain growth method, in which anisometric particles with sizes from several to a few tens micrometers are required (Kimura, 2006; Messing et. al., 2004; Tani & Kimura, 2006). The formation of aggregates must be avoided to form green compacts by tape-casting.

The requirements on the salt are that they are stable, readily available, inexpensive, and easily washed away with water. A low melting temperature is desirable, and the eutectic composition or the composition at the minimum liquidus temperature is often used. Other requirements are that they have a low vapor pressure at the heating temperature and do not cause undesirable reactions with either the reactants or the product. One example of unsuitable salt is LiCl, which is used for the preparation of $LiFe_5O_8$ (Wickham, 1971). LiCl accelerates the reaction between Fe_2O_3 and Li_2CO_3 to yield $LiFe_5O_8$, but it is hygroscopic and volatile at the reaction temperature. Furthermore, it is subject to hydrolysis; Li_2O produced by hydrolysis reacts with $LiFe_5O_8$ and converts it to $LiFeO_2$.

This chapter deals with (1) the phenomena occurring during synthesis; (2) the reaction rate; (3) the characteristics of powders with a special emphasis on particle morphology; and (4) the reaction of salt with the reactants and product. This chapter excludes (1) the salts as a reaction promoter; (2) the formation of simple oxides (MO); and (3) the salts as a reactant, such as the formation of $LiCoO_2$ and $LiMn_2O_4$ using Li salts (LiCl, $LiNO_3$, etc.), which is an important application of molten salt synthesis to lithium ion batteries (Han et al., 2003). Furthermore, this chapter does not include nitrate salts, because the reaction mechanisms are different from those of the chlorides and sulfates (Afanasiev & Geantet, 1998).

2. Fundamentals of molten salt synthesis

2.1 Preparation procedure

2.1.1 Formulation

Figure 1 shows the flowchart of the preparation procedure. A reaction batch contains the reactants and the salt. The salt is selected based on the desired powder characteristics. The

relation between the properties of the salt and the powder characteristics is described in this review. Sometimes, a surfactant is added to prepare nano-sized powders (Mao et al., 2003). In general, the mixing ratio of reactants is stoichiometric, i.e., two moles of Bi_2O_3 and three moles of TiO_2 are mixed for $Bi_4Ti_3O_{12}$. Care must be paid when carbonates are used as reactants. The solubility of oxides in the molten salt is generally low but that of carbonates is high, resulting in deviations from stoichiometry in the product phase. In the preparation of $Ba_6Ti_{17}O_{40}$, the Ba/Ti ratio of 6/17 in the reactant mixture results in the inclusion of $Ba_4Ti_{13}O_{30}$ particles in the product and that of 6/15 is employed to obtain nearly single-phase $Ba_6Ti_{17}O_{40}$ (Kimura, et al., 2005). When $KNbO_3$ is prepared from $K_4Nb_6O_{17}$ and K_2CO_3 using KCl, a K_2CO_3/ $K_4Nb_6O_{17}$ ratio of 1.2 or greater is desirable (Saito & Takao, 2007).

A typical amount of salt is 80-120 wt% of the reactant mixture. The amount is determined by the requirement that there is adequate salt to substantially fill the interstices of the reactant particles and to coat the reactant surfaces. In some systems, the amount of salt influences the product particle size (Yoon et al. 1998). When the amount of salt is too small, the effect of the liquid phase is not fully expected. An extremely large amount causes two problems. One is the separation of the reactant particles by sedimentation (Kimura et al., 1980; Wickham, 1971). When the reactant particles have different densities and sizes, they have different sedimentation rates, resulting in the separation of the reactant particles and a reduction in the reaction rate. Another problem is related to difficulties during treatment. When the amount of salt is excessive, the interstices of the reactant particles can never hold all of the molten salt, and a fairly large amount of the molten salt oozes from a gob of reactants. Oozed molten salt never acts as a solvent. Furthermore, the molten salt adheres to the wall of the crucible and changes to a hard lump after solidification. The dissolution of hard salt in the lumps is quite laborious.

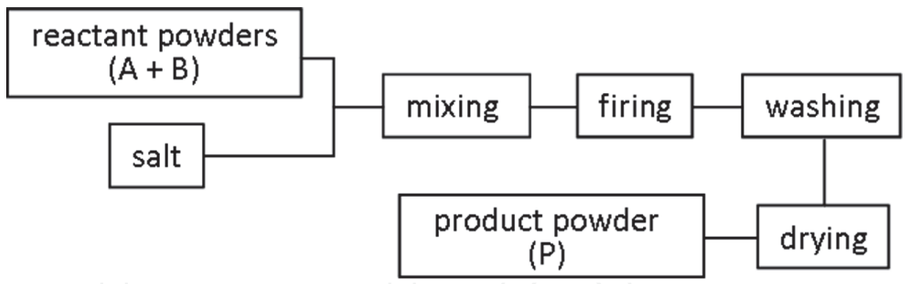

Fig. 1. Preparation procedure in molten salt synthesis.

When all the reactants are dissolved in the molten salt, another problem arises. It is related to the particle size. When Bi_2WO_6 is prepared from Bi_2O_3 and WO_3 using NaCl-KCl, two kinds of platelike particles are obtained depending on the amount of salt and the heating temperature (Kimura & Yamaguchi, 1982). The first kind consists of particles with a diameter of several micrometers, and the second kind of particles has a diameter of about 100 μm. When the amount of salt is small and the heating temperature is low, the system is located in the solid-liquid two-phase region of the phase diagram. The Bi_2WO_6 particles nucleate heterogeneously on the surfaces of the reactants, and a great number of them form. Conversely, when the amount of salt is large and the heating temperature is high, the system is located in the liquid single-phase region. The Bi_2WO_6 particles homogeneously nucleate in the liquid phase. Because the cooling rate is relatively high compared to that employed in the single-crystal growth, many nuclei form but the number of nuclei is less

than that nucleated heterogeneously on the surfaces of the reactants. Thus, quite large-sized particles are obtained.

2.1.2 Heat treatment

The mixture of reactants and salt is put in a covered or sealed crucible and heated in a furnace. A platinum crucible is used in the laboratory experiment. Alternatively, alumina and zirconia crucibles may be used if the chemical interaction between the crucible and the reactants and product is negligible. The heating conditions such as temperature and duration are determined by the desired powder characteristics. In general, the rate of material transport is increased with an increase in the heating temperature. At the same time, the salt evaporation increases as well. The heating duration is determined by the reaction rate and the size and shape of the product particles. Typical conditions are temperatures between 800°C and 1100°C with durations between 30 and 60 min. In a particular system, the heating rate influences the size of the product particles (Yoon et al., 1998).

After heating, the product mass is washed with an appropriate solvent to remove the salt. Ordinarily, this is water, which means that water-soluble salts are typically used in molten salt synthesis. The solubilities of chlorides and sulfates are generally high and washing with water two or three times seems sufficient to remove all the salt. Nevertheless, the ions from the dissolved salt may adsorb on the surfaces of the product particles, and, then, repeated washing is necessary. The chloride ions are sometimes detected by an Ag^+ solution even after ten times of washing. To desorb ions efficiently, the use of hot, instead of cold, water is recommended. After washing, the supernatant water is decanted and the remaining powder is dried. When the formation of hard agglomerates needs to be avoided, the powder is rinsed with a solvent with low surface tension, such as acetone, before drying.

2.2 Formation of product particles

2.2.1 Two stages of particle formation

The product particles are formed in two stages, which are the reaction and particle-growth stages (Kimura & Yamaguchi, 1983). In the reaction stage, the product particles are formed in the presence of solid reactant particles. The reactant particles dissolve in the molten salt and product particles form. When all the reactant particles are consumed, the particle-growth stage starts. There are solid product particles and molten salt in the system. The product particles have a particle size distribution, and the large particles increase their size by Ostwald ripening (Rahaman, 2003); particles smaller than a critical size dissolve in the molten salt and precipitate on the surfaces of particles larger than the critical size. The supersaturation with respect to the product compound is different in the two stages.

2.2.2 Supersaturation

The supersaturation is determined by the concentration of the reactants in the molten salt. When the product (P) is formed by a reaction between reactants A and B ($A + B \rightarrow P$), the solubility of P determines the equilibrium concentration of A and B in the molten salt, i.e., $[A]_e$ and $[B]_e$, respectively. The supersaturation is given by $([A][B]/[A]_e[B]_e - 1)$, where [A] and [B] are the actual concentration of A and B, respectively, in the molten salt. In the reaction stage, the solid reactant particles are present, and [A] and [B] are equal to their solubilities [A]* and [B]*, respectively. Figure 2 shows the relation between the molar free

energy of a liquid phase (G^l) and the composition of A (mole fraction) (Hillert, 1998). The chemical potential of the molten salt is indicated by μ_{salt}^l on the vertical axis at x_A=0, and μ_A^l and μ_A^s on the vertical axis at x_A=1 are the chemical potentials of liquid and solid A, respectively. The contact point of the G^l curve and the tangent line to G^l from μ_A^s (dashed straight line T_A in Fig. 2) gives the equilibrium concentration of A in the molten salt, which is the same as solubility of A ([A]*). Figure 2 does not show the relation for B, but the same relation applies. In the same manner, the equilibrium concentration of A in the molten salt coexisting with P is given as $[A]_e$, where the chemical potential of A in the solid P phase is indicated by $\mu_{A \text{ in } P}$ on the vertical axis at x_A=1. The difference between μ_A^s and $\mu_{A \text{ in } P}$ corresponds to the free energy change of the reaction $\Delta_r G$, because $\Delta_r G = (\mu_{A \text{ in } P} - \mu_A^s) + (\mu_{B \text{ in } P} - \mu_B^s)$. When the reaction proceeds spontaneously, $\Delta_r G < 0$ and $\mu_A^s > \mu_{A \text{ in } P}$, as shown in Fig. 2, and the solubility of A ([A]*) is larger than $[A]_e$. Therefore, in the reaction stage, the solid reactants A and B are present with molten salt, and the degree of supersaturation with respect to P is high because $[A]=[A]^*>[A]_e$. When the reaction between A and B is complete, the solid phase present in the system is only P, and [A] and [B] are reduced to $[A]_e$ and $[B]_e$, respectively. Therefore, the degree of supersaturation with respect to P decreases to almost zero in the particle-growth stage.

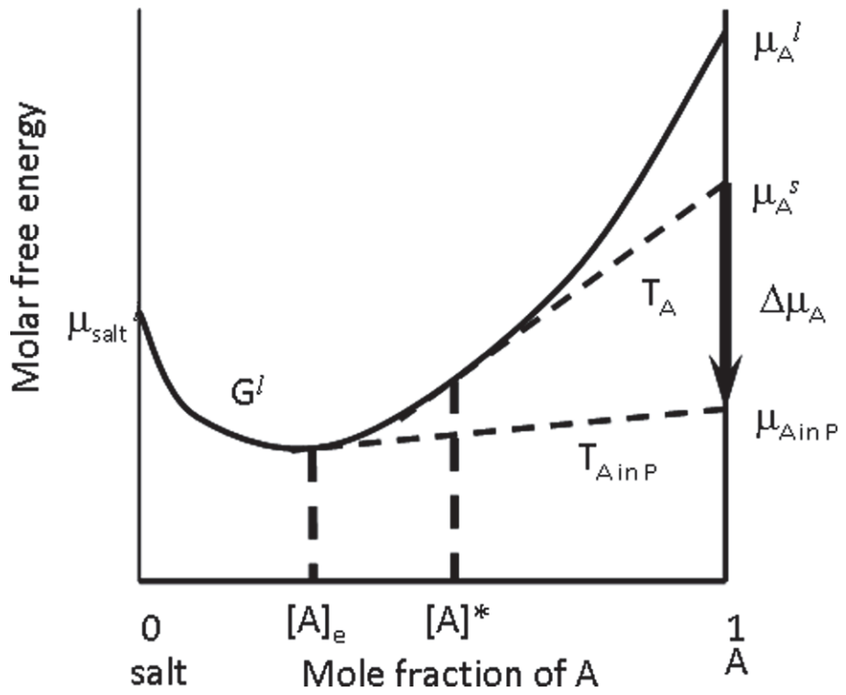

Fig. 2. Relation between the composition and the molar free energy of liquid phase.

Table 1 shows the solubility of $NiFe_2O_4$ and $ZnFe_2O_4$ in the chloride and sulfate salts together with that of NiO, ZnO, and Fe_2O_3. Irrespective of the salt species, the solubilities of ferrites are one order of magnitude smaller than those of the constituent oxides. The solubility is an important property in molten salt synthesis but the solubility data of oxides in molten salts are limited (Janz, 1967).

Oxides	Solubility (mol / g salt)			
	Sulfate salt*	NaCl	0.5NaCl-0.5KCl	KCl
NiO	1.6×10^{-6}	6.7×10^{-7}	6.7×10^{-7}	6.7×10^{-7}
ZnO	1.5×10^{-6}	1.7×10^{-6}	1.2×10^{-6}	9.1×10^{-7}
Fe_2O_3	4.8×10^{-6}	1.9×10^{-6}	2.2×10^{-6}	1.2×10^{-6}
$NiFe_2O_4$	5.1×10^{-7}	7.7×10^{-8}	9.8×10^{-8}	5.1×10^{-8}
$ZnFe_2O_4$	1.6×10^{-7}	2.4×10^{-7}	1.8×10^{-7}	5.0×10^{-8}

*: $0.635Li_2SO_4$-$0.365Na_2SO_4$

Table 1. Solubilities of $NiFe_2O_4$ and $ZnFe_2O_4$ and constituent oxides in salts at 900°C (Hayashi et al., 1986a)

2.3. Reaction rate

2.3.1 Reaction stage

Molten salts increase the reaction rate, and the product formation is completed at lower temperatures than that in solid state reaction. Figure 3 shows the fractional completion of the ferrite formation from the constituent oxides heated at various temperatures for 1 h in the solid state reaction and molten salt synthesis using Li_2SO_4-Na_2SO_4 (Takahashi et al., 1981). The molten salt decreases the temperature range of the reaction. Furthermore, three ferrites (M = Zn, Ni, and Mg) have almost the same temperature range in molten salt synthesis, whereas that largely depends on the chemical species of M in the solid state reaction.

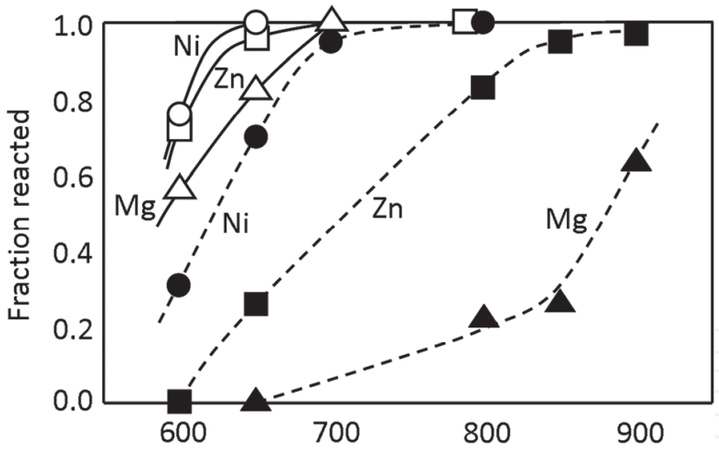

Fig. 3. Formation of MFe_2O_4 (M=Ni, Zn, Mg) with (solid lines) and without (dashed lines) molten Li_2SO_4-K_2SO_4 salt, heated for 1 h (Takahashi et al., 1981).

The promotion of reaction by molten salt has been reported in many systems. The increase in the formation rate is a consequence of (1) an increase in the contact area of the reactant particles and (2) an increase in the mobility of the reactant species in the molten salt (Arendt et al., 1979). The position of the product formation is limited to the contact points of the dissimilar reactants in the solid state reaction, and further increase in the product volume is caused by material transport through the product phase (Schmalzried, 1995). The mobility of material through this route is in the order of 10^{-18} cm^2 sec^{-1}. Conversely, in molten salt

synthesis, the surfaces of the reactant particles are covered with melt and they become available to the reaction. In the molten salt, the mobility of the species ranges from 10^{-5} to 10^{-8} cm^2 sec^{-1}. This is fairly larger than the mobility in the solid state reaction.

2.3.2 Particle-growth stage

After the reactants are completely consumed, the solid phase in the molten salt is only the product particles and the degree of supersaturation drops to almost zero. The prolonged heating increases the average particle size by Ostwald ripening. The rate of Ostwald ripening depends on the diffusion coefficient, the solubility, and the atomic structure of the particle surfaces (Rahaman, 2003). A large diffusion coefficient and solubility enhance the material transport in the molten salt. Therefore, a larger growth rate is expected at higher temperatures. The growth rate of surfaces with well-developed facets is low because of a smooth surface structure at the atomic scale (Kang et al., 2009). The effect of solubility on the growth rate is observed in the ferrite system. Prolonged heating of acicular $NiFe_2O_4$ and $ZnFe_2O_4$ particles in NaCl-KCl at 900°C causes the particles to adopt a somewhat rounded shape (Hayashi et al., 1986a). At this temperature, the formation reaction is complete in 4 min, and the particle shape is acicular. Therefore, the particles deform in the particle-growth stage. The degree of particle deformation is higher in $ZnFe_2O_4$ than $NiFe_2O_4$, for which the higher solubility of $ZnFe_2O_4$ than that of $NiFe_2O_4$ is responsible (Table 1). The same tendency is observed in $ZnFe_2O_4$ particles in NaCl, NaCl-KCl, and KCl. Use of NaCl results in a high degree of particle deformation. The solubility values are 2.4×10^{-7}, 1.8×10^{-7}, and 0.50×10^{-7} mol/g salt in NaCl, NaCl-KCl, and KCl, respectively (Table 1).

2.4 Powder characteristics

2.4.1 Homogeneity of composition

Molten salt enhances the material transport, and it is expected that the product powders are more homogeneous than those prepared by the solid state reaction. To examine the compositional homogeneity in $(Ni,Zn)Fe_2O_4$ powders, $NiFe_2O_4$ and $ZnFe_2O_4$ powders are reacted at 900°C for 4 h by molten salt synthesis using Li_2SO_4-Na_2SO_4 and by the solid state reaction. The compositional fluctuation in the obtained powders is analyzed by measuring the Curie temperature because it is a function of composition (Hayashi et al. 1985). Figure 4 shows the distribution of the Curie temperature for $(Ni,Zn)Fe_2O_4$ powders obtained by molten salt synthesis and solid state reaction. In the absence of molten salt, the distribution curve is broad, indicating a large compositional fluctuation. The molten salt narrows the distribution of the composition.

2.4.2 Agglomeration

During the solid state reaction, sintering (neck growth) of the product particles proceeds concurrently with their formation, which results in the formation of aggregates (Niesz & Bennett, 1978). In contrast, in molten salt synthesis, molten salt covers the surfaces of all particles present and prevents the formation of necks between the product particles. Therefore, it is expected that powders with a low degree of aggregation are obtained. Figure 5 shows the particle size distribution of rod-shaped $BaTiO_3$ particles obtained by the reaction between rod-shaped $TiO_2{\cdot}H_2O$ and $BaCO_3$ (Hayashi et al., 1986b). Heating temperatures are 700°C for the molten salt synthesis using NaCl-KCl and 1000°C for the

solid state reaction; these are minimum heating temperatures needed to complete the reaction within 1 h. The grain size of powder obtained by the molten salt synthesis is smaller than that obtained by the solid state reaction. Because the size of the primary particles is almost the same for both powders as observed with a scanning electron microscope, this size distribution reflects the size of the aggregates in the product powders. Thus, molten salt synthesis produces powders with a low degree of aggregation.

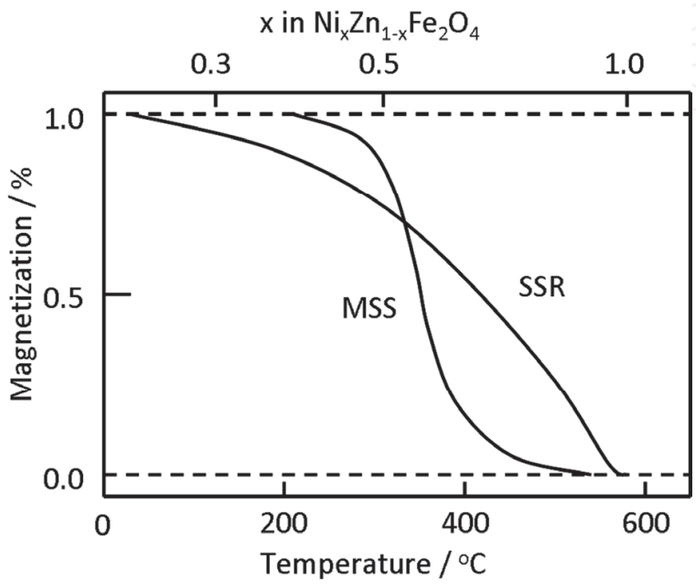

Fig. 4. Distribution of the Curie temperature in (Ni,Zn)Fe_2O_4 powders prepared by the molten salt synthesis (MSS) and solid state reaction (SSR), heated at 900°C for 4 h (Hayashi et al., 1985).

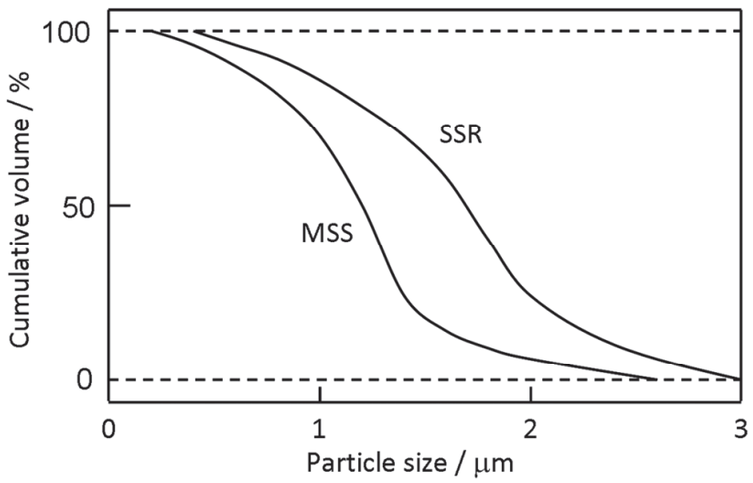

Fig. 5. Particle size distribution of $BaTiO_3$ powders obtained by the molten salt synthesis (MSS) and solid state reaction (SSR), measured by the sedimentation method (Hayashi et al., 1986b).

3. Morphology of powders

3.1 Equilibrium and growth forms

Powders with grains of various shapes are obtained by molten salt synthesis, depending on the chemical composition and reaction conditions. The presence of a liquid phase promotes the facet formation as usually observed in the single-crystal growth from solution (Elwell & Scheel, 1975). Because the crystal structure determines the crystallographic faces (*hkl*) of the stable facets, the particle shape is to some extent determined by the chemical composition. Powder particles are formed in two stages in molten salt synthesis. They are the reaction and particle-growth stages, and the supersaturation is high during the reaction stage and almost zero during the particle-growth stage (see **2.2**). Because the degree of supersaturation determines the growth rate of each crystallographic face, the particle shape is determined by the reaction conditions, such as the chemical species of the salt used, the reaction temperature and its duration, and the powder characteristics of the reactants.

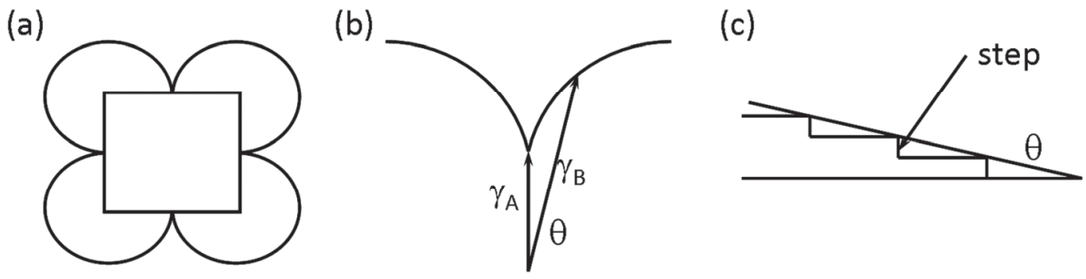

Fig. 6. The equilibrium form is derived from (a) the Wulff plot, (b) the depth of cusp is related to the value of surface free energies (γ_A and γ_B), and (c) the energy of steps on surface A is related to the difference $\gamma_B - \gamma_A$.

In general, the particle shape is determined by two factors, equilibrium and growth forms (Elwell & Scheel, 1975). The equilibrium form is the shape with the minimum surface free energy, and can be derived using the Wulff or γ plot. The Wulff plot is a polar diagram of the specific surface free energy, which is determined by the combination of solid and liquid materials. The equilibrium form is found by drawing all the planes normal to the radius vectors of the surface energy and taking the innermost envelop (Fig. 6(a)). A sharp cusp implies that a certain face has much lower free energy than other faces and the crystal will be facetted. The sharpness of the cusp in the γ plot relates to the roughness of the surfaces at the atomic scale. Figure 6(b) shows a part of the γ plot. Surface A has the lowest surface free energy of γ_A, and surface B is tilted by an angle θ and has a surface free energy of γ_B. The difference between γ_A and γ_B is the energy of the steps on the A surface (Fig. 6(c)). Therefore, a surface with a sharp cusp has high step energy; the density of steps on the surface with a well-developed facet is low.

The growth form is determined by the faces with the lowest growth rate in each direction (Elwell & Scheel, 1975). The growth rate of each face is determined by the structure of the surface at the atomic scale. It is generally anticipated in the crystal growth process that ions in the liquid phase adsorb on the crystal surface, diffuse over the surface, attach to a step on the surface, diffuse along the step, and finally are integrated into the crystal at a kink. When the surface is atomically rough, the density of steps and kinks is high, resulting in a high ion

integration rate into the crystal, and vice versa. Therefore, the surface with a well-developed facet has an atomically smooth structure and a low growth rate. The adsorption of the materials dissolved in a solvent or the solvent itself also influences the growth rate through changing the surface roughness or filling the growth sites.
The particle shape depends on the degree of supersaturation. In many cases, the growth rates of different faces exhibit different dependence on the degree of supersaturation. At a low degree of supersaturation, the difference in the growth rates is large and particles with a distinctive habit form. At a high degree of supersaturation, many faces have almost the same growth rate and particles with an equiaxed, rounded shape form.

3.2 Shape of particles during reaction stage

The degree of supersaturation changes in the course of reaction: it is high during the reaction stage and low during the particle-growth stage. Two mechanisms of particle formation are reported during the reaction stage, and Ostwald ripening is the main mechanism during the particle-growth stage. Powders with the desired morphology (size and shape) can be obtained by the precise control of the reaction conditions in these stages (Tiano et al., 2010).
Figure 7 shows the schematic diagram of the formation of product particle P from reactants A and B. The relative dissolution rate determines the dominant formation mechanism. When the dissolution rates of A and B are comparable (Fig. 7(a)), both reactants dissolve in the molten salt and the product particles precipitate under a high degree of supersaturation (solution-precipitation process: mechanism 1). In this case, particles have a growth form, which is often different from the equilibrium form. Typical examples are Bi_2WO_6 obtained from Bi_2O_3 and WO_3 using Li_2SO_4-Na_2SO_4 (Kimura & Yamaguchi, 1982) and $TiZrO_4$ from TiO_2 and ZrO_2 using KCl (Kimura et al., 1992). The Bi_2WO_6 and $TiZrO_4$ particles have rectangular and irregularly rounded shapes, whereas the equilibrium forms are an oblate an oblate sphere and needle, respectively.

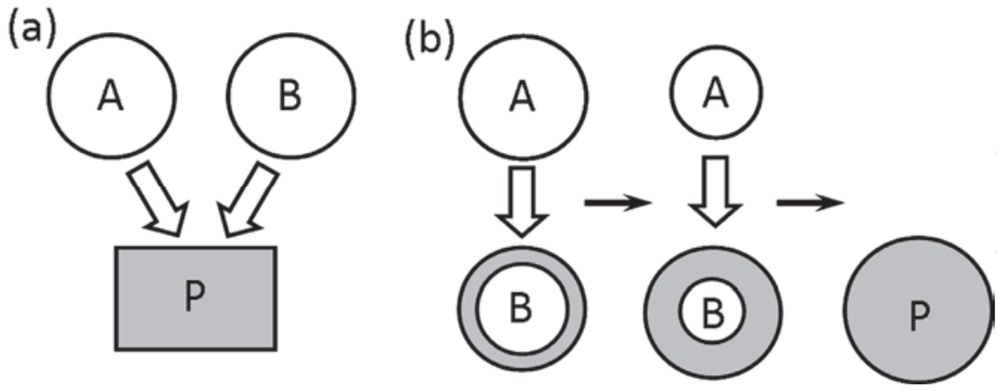

Fig. 7. Schematic diagrams of the formation of product particle P from reactant particles A and B by (a) solution-precipitation and (b) solution-diffusion processes.

When the dissolution rate of A is considerably higher than that of B, and the product layer forms on the surface of particle B (Fig. 7(b)), then another mechanism operates. The product layer prevents the dissolution of B. A large amount of A dissolves in the molten salt before the dissolution of B, diffuses through the molten salt, reaches the surface of particle B, and

reacts with B. The reaction proceeds by the diffusion of A from the interface of the molten salt/product layer to the interface of product layer/particle B and/or by the diffusion of B in the reverse direction, resulting in an increase in the thickness of the product layer. Finally, reactants A and B are completely consumed and the product particle with almost the same shape as that of particle B are obtained (solution-diffusion process: mechanism 2). Sometimes, this mechanism is called templating (Yang et al. 2001).

The relative dissolution rate is important because it determines the mechanism of the particle formation. It is determined by the solubility and particle size of the reactants. In the preparation of $LiFe_5O_8$ by the reaction between Li_2CO_3 and Fe_2O_3 in Li_2SO_4-Na_2SO_4 salt, Li_2CO_3 dissolves completely in the molten salt and $LiFe_5O_8$ particles form by the solution-diffusion process (mechanism 2) (Wickham, 1971). Acicular $NiFe_2O_4$ and $ZnFe_2O_4$ particles are prepared by the reaction between acicular Fe_2O_3 and equiaxed NiO and ZnO using NaCl-KCl and Li_2SO_4-Na_2SO_4 (Hayashi et al., 1986a). The particles obtained in the reaction stage (700°C for 1 h) are divided into two groups; one has the acicular shape and the other has a deformed shape with equiaxed grains of about 0.1 μm and rounded acicular particles. $ZnFe_2O_4$ obtained in NaCl-KCl and Li_2SO_4-Na_2SO_4 and $NiFe_2O_4$ obtained in NaCl-KCl have the acicular shape, whereas $NiFe_2O_4$ obtained in Li_2SO_4-Na_2SO_4 has the deformed one. The effect of the chemical species on the particle shape is explained by the solubility of ferrites in molten salt (Table 1). $NiFe_2O_4$ has the highest solubility in Li_2SO_4-Na_2SO_4 (5.1×10^{-7} mol/g salt) compared to $NiFe_2O_4$ in NaCl-KCl (0.98×10^{-7} mol/g salt) and $ZnFe_2O_4$ in Li_2SO_4-Na_2SO_4 and NaCl-KCl (1.6×10^{-7} and 1.8×10^{-7} mol/g salt, respectively). The possible explanation is that the high solubility of $NiFe_2O_4$ in Li_2SO_4-Na_2SO_4 requires an extensive time for saturation with $NiFe_2O_4$. This gives a greater opportunity for Fe_2O_3 to dissolve, and $NiFe_2O_4$ particles are formed by the solution-precipitation process (mechanism 1).

The relative dissolution rate is also determined by the size of the reactant particles. $NiFe_2O_4$ powders with different shapes are obtained by the reaction of the same Fe_2O_3 powder with two NiO powders with different sizes in Li_2SO_4-Na_2SO_4 (Kimura et al., 1980). In this case, the condition with respect to the solubility is the same, and the origin of the difference in particle shape is explained by the dissolution rate determined by the particle size. Figure 8 shows the shapes of the reactant Fe_2O_3 and product $NiFe_2O_4$ powders. The $NiFe_2O_4$ particles obtained by the reaction with fine NiO particles have almost the same shape as that of Fe_2O_3 particles, and those obtained by the reaction with coarse NiO particles have well-developed {111} facets. The dissolution rate of fine NiO particles is larger than that of Fe_2O_3 and the $NiFe_2O_4$ particles are formed by the solution-diffusion process (mechanism 2). In the case of coarse NiO particles, the solution-precipitation process (mechanism 1) is dominant and {111} facets develop; {111} is the closed packed planes of the spinel structure.

The evidence that the particle size determines the rate of dissolution in molten salt is reported in the formation of $(Ni,Zn)Fe_2O_4$ by the solution-precipitation process from $NiFe_2O_4$ and $ZnFe_2O_4$ with various particle sizes in the presence of Li_2SO_4-Na_2SO_4 (Hayashi et al., 1985). The mixtures of $NiFe_2O_4$ and $ZnFe_2O_4$ with various values of the fractional surface area of $NiFe_2O_4$ (surface area of $NiFe_2O_4$ in the starting mixture/total surface area of $NiFe_2O_4$ and $ZnFe_2O_4$ in the starting mixture) is heated at 900°C for 10 min, and the composition of the $(Ni,Zn)Fe_2O_4$ particles formed at the initial stage of the reaction is determined by the Curie temperature measurement. Figure 9 shows the relation between the fractional surface area of $NiFe_2O_4$ and the composition of the $(Ni,Zn)Fe_2O_4$ particles. A simple relation is observed, indicating that the dissolution rate is determined by the surface area, i.e., the particle size.

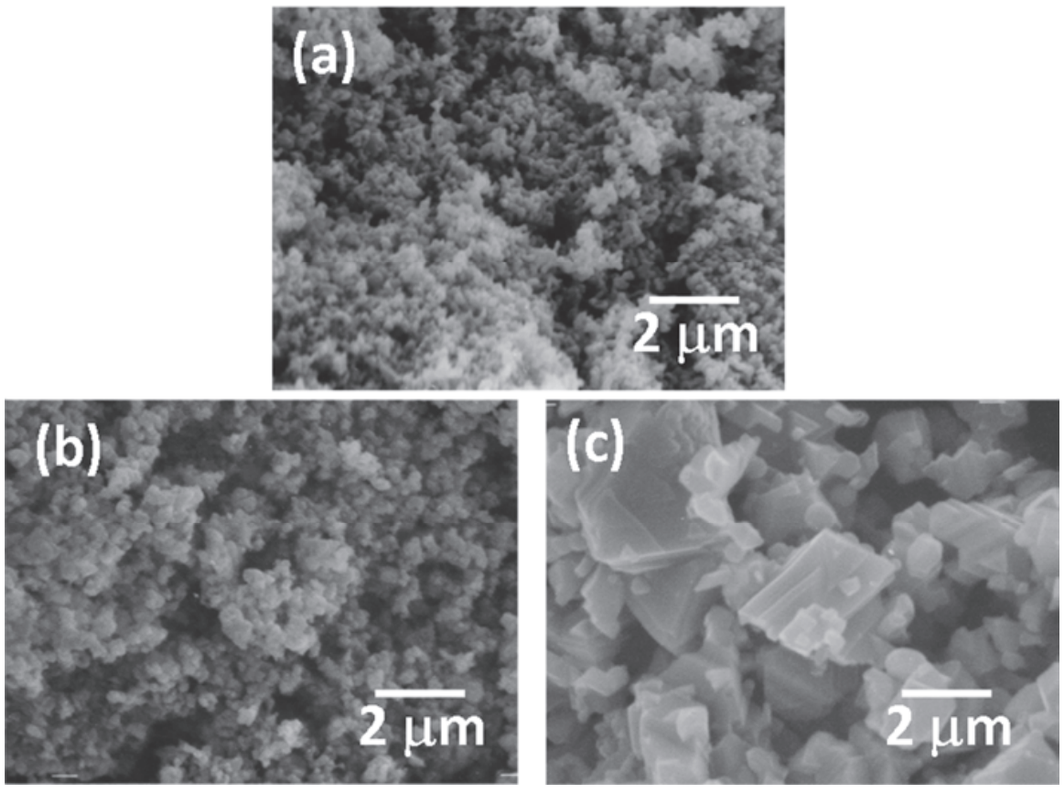

Fig. 8. Equiaxed and faceted $NiFe_2O_4$ particles ((b) and (c), respectively) are obtained from equiaxed Fe_2O_3 particles (a) by the reaction of fine and coarse NiO particles, respectively (Kimura et al., 1980).

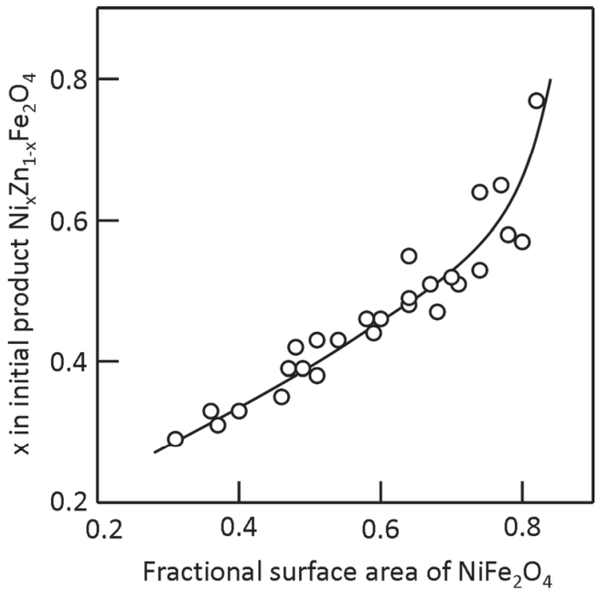

Fig. 9. The relative surface area of $NiFe_2O_4$ particles determines the Ni concentration in $(Ni,Zn)Fe_2O_4$ (Hayashi et al., 1985).

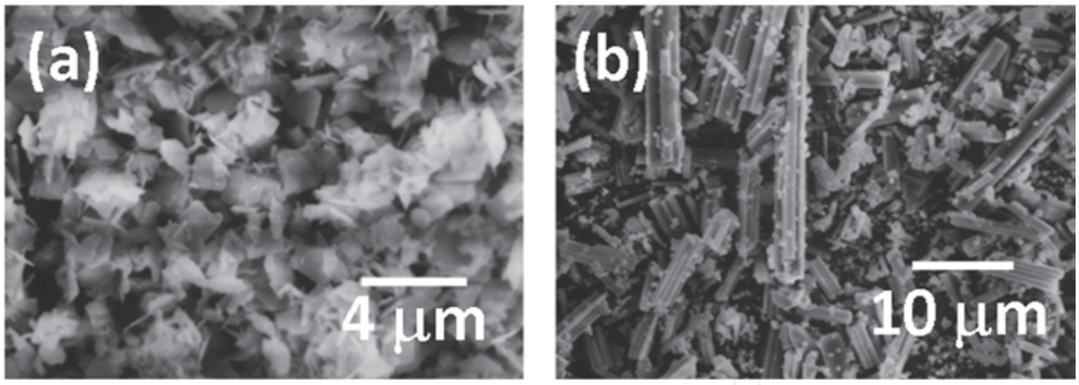

Fig. 10. Morphology of (a) $Bi_4Ti_3O_{12}$ and (b) $PbK_2Nb_5O_{15}$ particles obtained in the reaction stage (Kimura & Yamaguchi, 1983; Kimura et al. 1983a).

The degree of supersaturation is high when the product particles are formed by the solution-precipitation process (mechanism 1) and, consequently, aggregates often form. Figure 10 shows examples of aggregates (Kimura & Yamaguchi, 1983; Kimura et al. 1983a). $Bi_4Ti_3O_{12}$ and $KPb_2Nb_5O_{15}$ have platelike and needle-like shapes, respectively. The $Bi_4Ti_3O_{12}$ aggregates are composed of small platelike particles, and the $KPb_2Nb_5O_{15}$ aggregates have a columnar structure. In the latter case, discrete, needle-like particles are formed in the initial stage of the reaction, and a high degree of supersaturation causes the nucleation of new particles at particle edges as shown in Fig. 11.

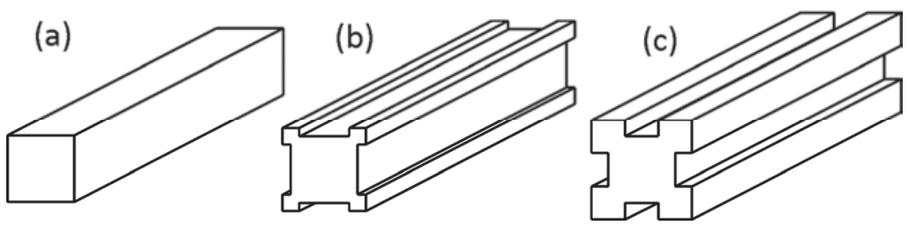

Fig. 11. Formation of the columnar structure by heterogeneous nucleation at the edges of needlelike particle.

3.3 Shape of particles during particle-growth stage

The free energy associated with the particle/molten-salt interfaces decreases during the particle-growth process via two routes. The first is the reduction of the surface area, resulting in particle growth. The second is the disappearance of surfaces with high energy, resulting in a shape change towards the equilibrium form.

The particle growth at this stage is caused by Ostwald ripening, and the growth rate is determined by the solubility and diffusion coefficient of the product oxide (Rahaman, 2003). Therefore, the heating temperature is a decisive factor in determining the particle size. For example, $Bi_4Ti_3O_{12}$ particles in KCl are platelike with the diameter of the plate faces of about 5 μm after heating at 950°C for 1 h and about 25 μm after 1 h at 1130°C, and the size can be controlled by selecting the heating temperature and its duration (Kimura & Yamaguchi, 1983). The exceptions are observed in highly faceted particles. The highly faceted surfaces have a high degree of smoothness at the atomic scale and high step energy, and their growth is sluggish (Kang et al., 2009). For example, platelike $BaBi_4Ti_4O_{15}$ particles in KCl hardly

grow in the particle-growth stage (Kimura & Yoshida, 2006). The top and side faces of the $BaBi_4Ti_4O_{15}$ particles are highly faceted; whereas the side faces of $Bi_4Ti_3O_{12}$ particles are atomically rough. The growth rate of the $BaBi_4Ti_4O_{15}$ particles is substantially zero. Therefore, the control of the particle size by selecting the heating conditions is difficult. Large $BaBi_4Ti_4O_{15}$ particles can be obtained from $Bi_4Ti_3O_{12}$ using the topochemical micro-crystalline conversion (see **3.4.1**) (Kimura & Yoshida, 2006).

If the surfaces of the particles formed in the reaction stage have higher interfacial energy than those of the equilibrium form, the particle shape changes to reduce the total interfacial energy. A typical example is Bi_2WO_6 obtained from Bi_2O_3 and WO_3 in Li_2SO_4-Na_2SO_4 (Kimura & Yamaguchi, 1982). The shape of the Bi_2WO_6 particles in the reaction stage is rectangular and changes to oblate in the particle-growth stage. Bi_2WO_6 has a layered structure and platelike particles form in NaCl-KCl in the reaction and particle-growth stages. The (001) cusp is sharp in NaCl-KCl and shallow in Li_2SO_4-Na_2SO_4, as expected from their shapes in the particle-growth stage. The shallow cusp indicates that the step energy on the (001) face is low and the growth rate of (001) is not different from that of other faces. Thus, the (100), (010), and (001) faces have almost the same growth rate under a high degree of supersaturation (reaction stage), resulting in the rectangular shape. In the particle-growth stage, either the particle shape approaches the equilibrium form or the growth rate of (001) becomes smaller than that of (100) and (010) under a low degree of supersaturation. The dependence of particle shape on the degree of supersaturation is also observed in the cases of $NiFe_2O_4$ (Kimura et al., 1980) and $BaZrO_3$ (Zhou et al., 2007).

The aggregated $Bi_4Ti_3O_{12}$ particles formed in the reaction stage (Fig. 10(a)) change to discrete platelike particles in the particle-growth stage (Kimura & Yamaguchi, 1983). The particle shape is shown in Fig. 12(a). However, the aggregated $KPb_2Nb_5O_{15}$ particles with a columnar structure (Fig. 10(b)) do not change their shape by prolonged heating, because the particle surfaces are highly faceted. Therefore, the discrete needle-like particles are obtained via a different route (Kimura et al. 1983a). The formation of particles with a columnar structure must be avoided. Therefore, the degree of supersaturation must be kept low in the reaction stage. A mixture of PbO, Nb_2O_5, and KCl is heated at 750°C for 1 h. The obtained material is $PbNb_2O_6$ powder composed of aggregates of small equiaxed particles. Then, the material is heated at 1050°C for 3 h. The reaction with KCl change the particles from $PbNb_2O_6$ to $KPb_2Nb_5O_{15}$ (see **4.1**), and the growth at a low degree of supersaturation results in the formation of discrete needle-like particles (Fig. 12(b)).

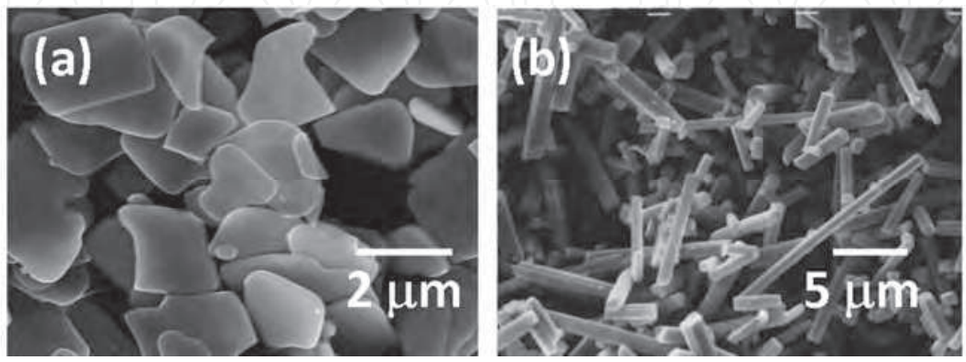

Fig. 12. Morphology of (a) $Bi_4Ti_3O_{12}$ and (b) $PbK_2Nb_5O_{15}$ particles obtained in the particle-growth stage (Kimura & Yamaguchi, 1983; Kimura et al. 1983a).

A change in the particle shape as a function of the heating temperature is reported for $SrO{\cdot}5.5Fe_2O_3$ from Fe_2O_3 and $SrCO_3$ in KCl (Park et al., 1996). Heating at 900°C results in the formation of platelike particles and that at 1200°C produces near-spherical particles. The origin of this shape change is the change in the surface structure from smooth to rough at the atomic scale. The smooth surfaces have high step energy and develop the facets, leading to the platelike shape. The various crystallographic faces on the rough surfaces have almost the same growth rate, resulting in the near-spherical shape. The rate-determining step is also changed from reaction-controlled to diffusion-controlled. The particle size is not largely dependent on the amount of salt for the reaction-controlled case, whereas the mean particle size decreases as the amount of salt is increased in the diffusion-controlled case.
The particle shape obtained via the molten salt synthesis can be predicted from the crystal structure of the product, but the prediction is not always successful because the chemical species of the salt also influence the particle shape, because the γ-plot (Fig. 6(a)) is determined by the combination of the product and salt materials. The particle shape is often determined in the particle-growth stage with a low degree of supersaturation. The growth under a low degree of supersaturation is similar to that in the single-crystal growth from solution. Therefore, the reported shape of single crystals can be used to predict the shape of particles obtained via the molten salt synthesis (Elwell & Scheel, 1975).

3.4 Topochemical micro-crystalline conversion

In materials with low crystallographic symmetry, particles with an anisometric shape can be easily prepared by molten salt synthesis. In contrast, for materials with high crystallographic symmetry, particles with a large aspect ratio (plate or needle) are difficult to prepare directly from the constituent materials, because this shape is far from the equilibrium form. In this case, a precursor particle is used and, subsequently, it is converted to the objective material. The precursor particle must have an anisometric shape and a topotactic relation with the objective material. Molten salt synthesis can easily make the solution-diffusion mechanism dominant (mechanism 2 in Fig. 7); the particles of the objective material are formed by the diffusion of the supplementary material into the precursor particles, thus, preserving the outer shape of the precursor particles. This method is called topochemical micro-crystalline conversion, and is divided into three groups based on the relation between the crystal structures of the precursor and the objective materials; (1) the precursor with a structure similar to the objective material; (2) the precursor with a structure different from the objective material; and (3) the conversion accompanied by by-product.

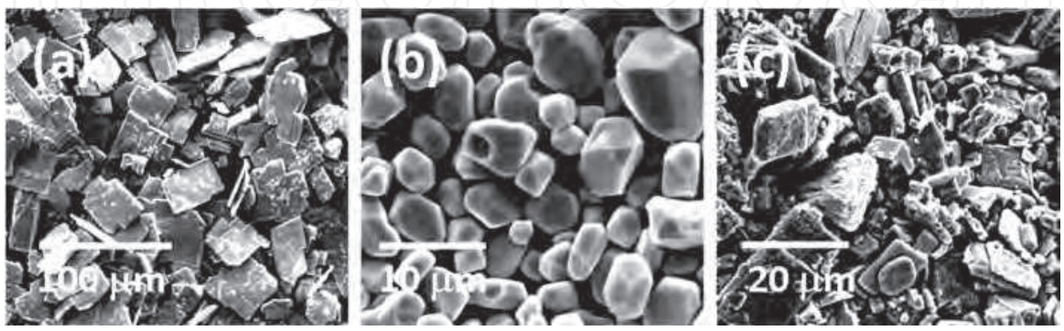

Fig. 13. Morphology of (a) platelike $K_4Nb_6O_{17}$, and (b) equiaxed and (c) platelike KNb_2O_6 particles (Sakurai, 2011).

The shape of the precursor particles must be preserved during the topochemical reaction, which occurs in the reaction stage (see **3.2**). In the reaction stage, two reaction processes are possible; the solution-precipitation and solution-diffusion processes. If the former process is dominant, the precursor particles dissolve and the objective material particles precipitate with an intrinsic shape. Therefore, anisometric particles cannot be obtained. The reaction conditions must be selected to make the solution-diffusion process dominant. Platelike $KNbO_3$ particles are obtained via platelike $K_4Nb_6O_{17}$ particles (Saito & Takao, 2007). Figure 13(a) shows platelike $K_4Nb_6O_{17}$ particles obtained by the reaction between Nb_2O_5 and $(COOK)_2{\cdot}H_2O$ in KCl. $KNbO_3$ is obtained by the reaction of the platelike $K_4Nb_6O_{17}$ particles with $(COOK)_2{\cdot}H_2O$, but the particle shape depends on the particle size of (COOK)2·H2O (Sakurai, 2011). When $(COOK)_2{\cdot}H_2O$ particles of tens of micrometer are used, $KNbO_3$ particles with an equiaxed shape are obtained (Fig. 13(b)). When $(COOK)_2{\cdot}H_2O$ particles of several micrometers are used, then, polycrystalline platelike particles are obtained (Fig. 13(c)). The $(COOK)_2{\cdot}H_2O$ particle size determines the dissolution rate of K_2O in the molten salt and the process of the formation of the $KNbO_3$ particles. Usually, K_2CO_3 is used as the potassium source, but it is hygroscopic and difficult in handling. $(COOK)_2{\cdot}H_2O$ is not hygroscopic and it can be used in the preparation of the particles (Fig. 13); $(COOK)_2{\cdot}H_2O$ decomposes to K_2CO_3 upon heating at about 370°C.

The chemical species of the reactants also determine the reaction process. In the preparation of $PbTiO_3$ in NaCl-KCl, the $PbTiO_3$ particle shape depends on the titanium source (Cai et al., 2007). Needlelike $PbTiO_3$ particles are obtained from needlelike TiO_2 particles, whereas the use of needlelike $K_2Ti_4O_9$ particles results in the formation of cube-shaped $PbTiO_3$ particles. When the needlelike TiO_2 particles are used, the dominant process of the $PbTiO_3$ formation is solution-diffusion (mechanism 2). In the $K_2Ti_4O_9$ case, the needlelike $K_2Ti_4O_9$ particles break-up to small pieces before reacting with PbO, or the reaction in the reaction stage is caused by the solution-precipitation process (mechanism 1). A similar effect of the source of the B-site cation is reported for $ANbO_3$ (A = Na, K, and (Na,K)) (Li et al., 2009). The effect of the barium source is seen in the preparation of needlelike $BaTiO_3$ particles (Huang et al., 2009). $BaCO_3$ gives needlelike $BaTiO_3$ particles via the reaction with the needlelike TiO_2 particles, but BaO produces cube-shaped $BaTiO_3$ particles. $BaCO_3$ has a high solubility and the $BaTiO_3$ particles are formed by the solution-diffusion process (mechanism 1 in Fig. 7), whereas the low solubility of BaO makes the solution-precipitation process dominant (mechanism 2 in Fig. 7).

3.4.1 Similar structures between precursors and products

The Aurivillius structure consists of alternately stacked Bi_2O_2 layers and pseudoperovskite blocks. The number of pseudoperovskite blocks is three in $Bi_4Ti_3O_{12}$ and four in $MBi_4Ti_4O_{15}$ (M = Ca, Sr, and Ba) (Fig. 14). The platelike $Bi_4Ti_3O_{12}$ particles are easily obtained by molten salt synthesis using KCl and their size can be easily controlled by selecting the heating temperature and duration. The growth rate of $BaBi_4Ti_4O_{15}$ is low and it is difficult to obtain platelike $BaBi_4Ti_4O_{15}$ particles with a diameter more than 10 μm (see **3.3**). The reaction of platelike $Bi_4Ti_3O_{12}$ particles with $BaTiO_3$ or $BaCO_3$ + TiO_2 in salt (for example, KCl-$BaCl_2$) results in platelike $BaBi_4Ti_4O_{15}$ particles with almost the same size as that of $Bi_4Ti_3O_{12}$ particles (Kimura & Yoshida, 2006). Because the addition of pseudoperovskite blocks into $Bi_4Ti_3O_{12}$ does not disturb the structure, single-crystalline $BaBi_4Ti_4O_{15}$ particles are obtained.

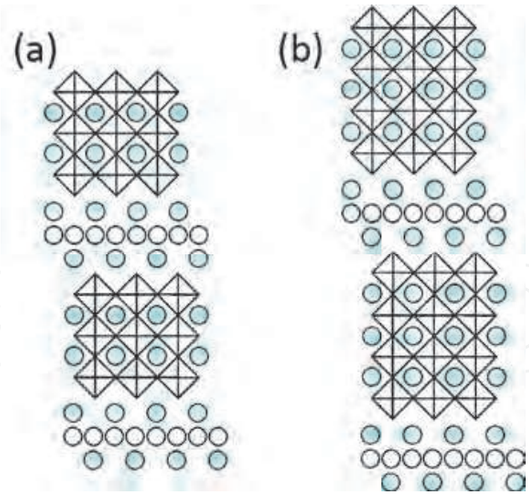

Fig. 14. Crystal structures of (a) $Bi_4Ti_3O_{12}$ and (b) $BaBi_4Ti_4O_{15}$.

3.4.2 Different structures between precursors and products

A material with a different crystal structure from the objective material can be used as a precursor, when the material has a topotactic relation to the objective material. Typical examples are the conversion of the layered perovskite to perovskite (Schaak & Mallouk, 2000) and the preservation of the packing direction of closed-packed layers. The former example is the formation of $SrTiO_3$ from $Sr_3Ti_2O_7$ and the latter of MFe_2O_4 (M = Zn, Ni, Mn, etc.) from α-Fe_2O_3 and of $BaTiO_3$ from $Ba_6Ti_{17}O_{40}$.

Tabular $SrTiO_3$ is obtained via a reaction between tabular $Sr_3Ti_2O_7$ and equiaxed TiO_2 in molten KCl (Watari et al., 2000). $Sr_3Ti_2O_7$ has a Ruddlesden-Popper-type layered perovskite structure, and tabular particles can be obtained by the reaction of $SrCO_3$ and TiO_2 in KCl. $Sr_3Ti_2O_7$ and $SrTiO_3$ have a topotactic relationship, $[001]_{Sr3Ti2O7}//[001]_{SrTiO3}$ and $[100]_{Sr3Ti2O7}//[100]_{SrTiO3}$, as shown in Fig. 15. The diffusion of reactant TiO_2 into the $Sr_3Ti_2O_7$ particles results in the formation of $SrTiO_3$ particles with the shape same as that of $Sr_3Ti_2O_7$ (Liu et al., 2009). Thus, tabular $SrTiO_3$ particles with [001] perpendicular to the tabular faces are obtained. In this case, both $Sr_3Ti_2O_7$ and $SrTiO_3$ particles are single crystals. A similar method is applied to the preparation of platelike $Bi_{0.5}Na_{0.5}TiO_3$ powders from platelike $Na_{0.5}Bi_{4.5}Ti_4O_{15}$ particles by the reaction $Na_{0.5}Bi_{4.5}Ti_4O_{15}+Na_2CO_3+TiO_2$ in NaCl (Zeng et al., 2006). $Na_{0.5}Bi_{4.5}Ti_4O_{15}$ and $Bi_{0.5}Na_{0.5}TiO_3$ have the Aurivillius (Fig. 14(b)) and perovskite (Fig. 15(b)) structure, respectively. In this case, the single-crystalline $Na_{0.5}Bi_{4.5}Ti_4O_{15}$ particles are converted to polycrystalline $Bi_{0.5}Na_{0.5}TiO_3$ particles.

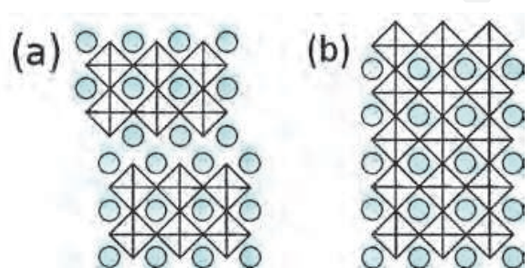

Fig. 15. Crystal structures of (a) $Sr_3Ti_2O_7$ and (b) $SrTiO_3$.

Alfa-Fe_2O_3 and MFe_2O_4 (M = Zn, Ni, Mn, etc.) have the corundum and spinel structure, respectively. They have closed-packed oxygen layers with different sequences; hexagonal (ABAB…) in Fe_2O_3 and cubic (ABCABC…) in MFe_2O_4. The directions perpendicular to these layers are preserved when MFe_2O_4 is formed by the diffusion of MO into Fe_2O_3. When platelike Fe_2O_3 particles prepared by the hydrothermal method are used, platelike MFe_2O_4 particles are obtained in Li_2SO_4-Na_2SO_4 (Kimura et al., 1981). In this case, platelike Fe_2O_3 particles are single crystals but the obtained MFe_2O_4 particles are polycrystalline, and the topotactic relationship is preserved in each grain, i.e., $[0001]_{Fe2O3}//[111]_{MFe2O4}$. Thus, platelike MFe_2O_4 particles with [111] perpendicular to the plate faces are obtained. By a similar process, needlelike $(Ni,Zn)Fe_2O_4$ particles are obtained from needlelike α-Fe_2O_3 (Hayashi et al., 1986a). Even though the orientation of $MgAl_2O_4$ crystal axes is not reported, platelike $MgAl_2O_4$ particles are obtained from platelike α-Al_2O_3 particles (Jayaseelan et al., 2007).

Similar preservation of the closed-packed layers is observed in titanates. $Ba_6Ti_{17}O_{40}$ and $BaTiO_3$ have closed packed layers containing both barium and oxygen ions. The packing sequences are hexagonal in $Ba_6Ti_{17}O_{40}$ (Hofmeister et al., 1984) and cubic in $BaTiO_3$. Platelike $Ba_6Ti_{17}O_{40}$ particles with the [001] direction perpendicular to the plate face (the crystal structure of $Ba_6Ti_{17}O_{40}$ is monoclinic) are obtained by the reaction of $BaTiO_3$ and TiO_2 in NaCl (Kimura et al., 2005), and they are converted into platelike $BaTiO_3$ particles with [111] perpendicular to the plate face by the reaction with $BaCO_3$ in NaCl (Sato & Kimura, 2008). In this case, the obtained platelike $BaTiO_3$ particles are polycrystals.

A series of topochemical reactions are employed to obtain anisometric particles. An example is needlelike $BaTiO_3$ (Hayashi et al., 1986b). At first, needlelike $K_2Ti_4O_9$ particles are prepared from K_2CO_3 and TiO_2 in K_2MoO_4 flux, converted to needlelike $TiO_2 \cdot nH_2O$ by washing with an HCl solution and to needlelike TiO_2 by heating at high temperatures, and finally reacted with $BaCO_3$ in NaCl-KCl. A similar procedure is employed to prepare needlelike and platelike $KNbO_3$ particles (Li et al., 2009).

3.4.3 Conversion accompanied by by-products

Platelike particles with the perovskite structure are prepared from platelike particles with the Aurivillius structure, as already shown for platelike $Bi_{0.5}Na_{0.5}TiO_3$ particles in **3.4.2** (Zeng et al., 2006). The Aurivillius structure shown in Fig. 14 consists of pseudoperovskite blocks and can be topotactically converted to the perovskite structure (Fig. 15(b)). To extend the method to other perovskite materials, the formation of Bi_2O_3 particles cannot be avoided as shown by the following reaction.

$$Bi_{2.5}Na_{3.5}Nb_5O_{18} + Na_2CO_3 \rightarrow NaNbO_3 + Bi_2O_3 + CO_2$$

Thus, platelike $NaNbO_3$ particles with [001] perpendicular to the plate faces are prepared from platelike $Bi_{2.5}Na_{3.5}Nb_5O_{18}$ particles, which are obtained by the reaction between Bi_2O_3, Na_2CO_3, and Nb_2O_5 in NaCl (Sait et al., 2004). The platelike $Bi_{2.5}Na_{3.5}Nb_5O_{18}$ particles are single crystals but change to polycrystalline $NaNbO_3$ particles. The by-product Bi_2O_3 particles cannot be removed by washing with water. Washing with an acid solution is necessary. Platelike particles such as BaTiO3 (Liu et al., 2007), CaTiO3 (Saito et al. 2008), PbTiO3 (Poterala et al., 2010), $SrTiO_3$ (Saito & Takao, 2006), $Bi_{0.5}Na_{0.5}TiO_3$ (Zhao et al., 2008), etc., can be prepared by the same procedure from appropriate precursors.

The mechanism of the topochemical conversion from the Aurivillius to the perovskite structure has been proposed by Poterala et al. (Poterala et al., 2010). The Aurivillius phase converts directly to the perovskite phase as in $NaNbO_3$ or via an intermediate phase, which is formed by multiple nucleations on the Aurivillius phase, as in $BaTiO_3$ and $PbTiO_3$. The conversion occurs in two sequential stages. The first stage is the multiple topotactic nucleation of the perovskite phase either directly on the Aurivillius phase or on the intermediate phase. The nuclei grow to small crystallites. They are slightly misaligned from the Aurivillius parent structure. At the end of the first stage, the Aurivillius single-crystal particle changes to an aggregate of aligned perovskite crystallites with a slight misorientation. In the second stage, the aligned crystallites in the aggregate grow to form a dense platelike particle. When the growth of the aligned crystallites is complete, the perovskite particles are single-crystals with almost the same shape and size as those of the Aurivillius particles. When the growth is incomplete, the perovskite particles are polycrystalline in nature. The change from single-crystalline, platelike $Bi_4Ti_3O_{12}$ particles to single-crystalline, platelike $Bi_{0.5}Na_{0.5}TiO_3$ particles via poly-crystalline, platelike aggregates is also observed in the stage of the template particle formation in $Bi_{0.5}Na_{0.5}TiO_3$ textured by the reactive-templated grain growth process (Motohashi & Kimura, 2008).

4. Reaction between oxides and salts

4.1 Reaction

It is desirable that salt acts as a pure solvent and does not react with the reactant and product materials. However, many reactions between oxides and salts (chlorides, sulfates, carbonates, etc.) are reported. Therefore, care must be taken to avoid the reaction with the salt in the selection of salt species.

Severe reactions are reported in the molten salt synthesis of niobates with the tungsten bronze structure. In the preparation of $PbNb_2O_6$ from PbO and Nb_2O_5, pure $PbNb_2O_6$ cannot be obtained using NaCl and KCl (Kimura et al., 1983b). When KCl is used as the molten salt, K ions extensively substitute for Pb ions and the product is a solid solution $(1-x)PbNb_2O_6$-$xKPb_2Nb_5O_{15}$ with the tungsten bronze structure. The extent of the substitution, x, is determined by the heating conditions. When NaCl is used, the substitution reaction proceeds to form the $(Na,Pb)NbO_3$ phase as well as $(1-x)PbNb_2O_6$-$xNaPb_2Nb_5O_{15}$. The reaction $PbO+2MCl \rightarrow M_2O+PbCl_2$ (M=Na, K) is responsible for this substitution.

Alkali chlorides cannot be used to prepare MNb_2O_6 (M=alkaline earth metal), and MCl_2 is a candidate for molten salt. When the product phase is the $M_xM'_{1-x}Nb_2O_6$ solid solution and the salt is MCl_2-$M'Cl_2$, then, an interchange reaction is possible. When $Sr_{0.5}Ba_{0.5}Nb_2O_6$ is prepared from $SrCO_3$, $BaCO_3$, and Nb_2O_5 using $SrCl_2$-$BaCl_2$, Sr–rich $(Sr,Ba)Nb_2O_6$ phase forms, for which the reaction $BaO+SrCl_2 \rightarrow BaCl_2+SrO$ is responsible (Furubayashi & Kimura, 2011). $Sr_{0.5}Ba_{0.5}Nb_2O_6$ can be prepared by selecting the $SrCl_2$ to $BaCl_2$ ratio.

The reaction between the Aurivillius phase and chloride is possible (Fuse, 2006). The Aurivillius phase has the general formula $Bi_2O_2(A_{m-1}B_mO_{3m+1})$, and a compound with an m value different form that of the objective material often forms. Figure 16 shows the X-ray diffraction patterns of $Bi_4Ti_3O_{12}$ obtained from Bi_2O_3 and TiO_2. When NaCl is used as the molten salt, the diffraction lines of $Na_{0.5}Bi_{8.5}Ti_7O_{27}$ are detected in the specimen heated at 1130°C. The diffraction lines other than those of $Bi_4Ti_3O_{12}$ are not detected in the specimens

heated at 950°C in NaCl and at 1130°C in KCl. $Bi_4T_3O_{12}$ reacts with NaCl at high temperatures but does not with KCl. The NaCl-KCl salt cannot be used in the preparation of $Bi_4Ti_3O_{12}$ at high temperatures. Because the Aurivillius compounds with different *m* values have similar X-ray diffraction patterns, close examination of the pattern is necessary to ensure the formation of the material with the desired composition (Sanson & Whatmore 2005).

The reactivity of an oxide with the salt often depends on the oxide chemical species. When Li_2SO_4 is used in the preparation of $BaFe_{12}O_{19}$ from $BaCO_3$ and Fe_2O_3, $LiFe_5O_8$ forms by the following reaction; $BaCO_3+5Fe_2O_5+Li_2SO_4 \rightarrow 2LiFe_5O_8+BaSO_4+CO_2$ (Wickham, 1971). The exchange reaction $MgCO_3+Li_2SO_4 \rightarrow MgSO_4+Li_2CO_3$ does not occur and $MgFe_2O_4$ is obtained from $MgCO_3$ and Fe_2O_3 in Li_2SO_4-Na_2SO_4.

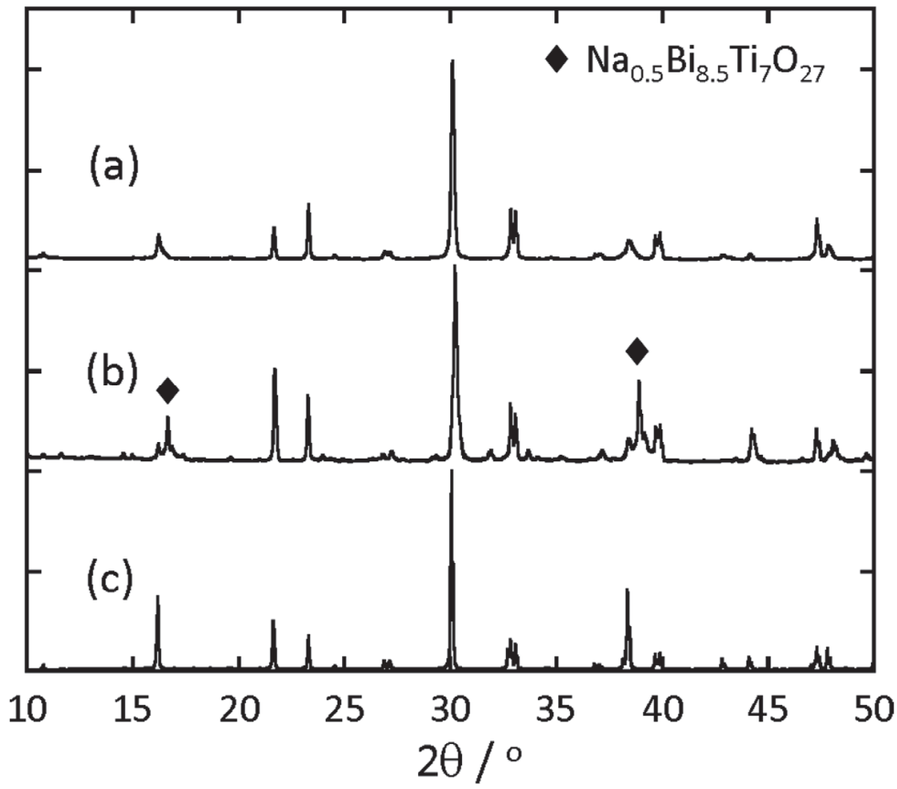

Fig. 16. X-ray diffraction patterns of the products of reaction $2Bi_2O_3+3TiO_2$ after 1 h (a) in NaCl at 900°C, (b) in NaCl at 1130°C, and (c) in KCl at 1130°C.

4.2 Positive uses of exchange reactions

The substitution reaction of alkali ions for alkaline earth ions is positively used for the preparation of needlelike $AM_2Nb_5O_{15}$ particles, where A and M are alkali and alkaline earth ions, respectively. When the $KSr_2Nb_5O_{15}$ particles are prepared from K_2CO_3, $SrCO_3$, and Nb_2O_5 using molten KCl, needlelike particles are obtained, but their size range is limited. The high degree of supersaturation during the reaction stage results in a large number of nuclei and the atomically smooth surfaces make the growth rate substantially zero. If the degree of supersaturation is low during the reaction stage, the number of nuclei is limited

and the formation of large needlelike particles is expected. When $SrCO_3$+Nb_2O_5 or $SrNb_2O_6$(+Nb_2O_5) is used as the reactant and an excessive amount of KCl is used as salt, needlelike $KSr_2Nb_5O_{15}$ particles of large size are obtained (Zhao et al., 2005; Yang et al., 2007).

Interesting ion-exchange reaction between the solid oxide and molten chloride is reported in the preparation of $RbCa_2Nb_3O_{10}$ at 800°C (Geselbracht et al, 2002). The reaction of K_2CO_3, $CaCO_3$, and Nb_2O_5 with a large excess of RbCl produces $RbCa_2Nb_3O_{10}$. K_2CO_3 is a necessary compound to form $RbCa_2Nb_3O_{10}$, because the reaction without K_2CO_3 results in the formation of $CaNb_2O_6$ and $Ca_2Nb_2O_7$. Heating $KCa_2Nb_3O_{10}$ in molten RbCl forms $RbCa_2Nb_3O_{10}$. These results indicate that the ion-exchange reaction is necessary to obtain $RbCa_2Nb_3O_{10}$.

5. Summary

Molten salt synthesis is a simple method for the preparation of ceramic powders. The preparation procedure is quite similar to that used in an ordinary powder metallurgical method. A mixture of reactant and salt powders is heated at temperatures above the melting point of the salt. The reactants interact under the presence of the molten salt. After a pre-determined heating stage, the product mass is cooled, and washed with a solvent (mainly water) to remove the salt. The product powder is obtained after drying.

The product powder is formed in two stages, reaction and particle-growth. In the reaction stage, the molten salt does not dissolve all the reactant powders and the reaction occurs in the presence of solid reactant particles. The product powder is formed by two processes under a high degree of supersaturation. One is the solution-precipitation process; all members of reactants dissolve in the molten salt and the product particles precipitate. Another is the solution-diffusion process; one of the reactants dissolves in the molten salt and reacts with another reactant on the surface of the latter. At the end of the reaction stage, the only solid material in the molten salt is the product particles. Further heating starts the particle-growth stage; the product particles change their size and shape under a low degree of supersaturation.

Powders of various sizes from a few tens nanometers to a few tens micrometers can be obtained by the careful control of the preparation conditions. The particle shape can also be controlled. The size and shape of particles changes in the course of the stages of particle formation. In the reaction stage, two types of particles can be obtained. When the product particles are formed by the solution-precipitation and solution-diffusion processes, the particles have a growth form and a shape similar to that of one of the reactant particles, respectively. The dominant process is determined by the relative dissolution rate of the reactant particles into the molten salt, and the dissolution rate is determined by the solubility and particle size of the reactant. In the particle-growth stage, the particle size is increased and the particle shape approaches the equilibrium form. For the materials with low crystallographic symmetry, anisometric particles can be obtained. When anisometric particles are desired for materials with high symmetry, the topochemical micro-crystalline conversion can be applied.

The application of molten salt synthesis is widely spread since 2005, from ferroelectric and ferromagnetic materials to materials for Li-ion batteries (Santhanam & Rambabu, 2010),

semiconductors (Huang et al, 2010), phosphors (Yan & Lei, 2010), and photocatalysts (Arney et al., 2008), especially with regard to nano-sized materials (Mao et al., 2007). Although this review only deals with complex oxides, the application has been extended to simple oxide powders with specific morphology (Tiano et al., 2010). The preparation of nanoparticles with various shapes (equiaxed, wire, strip, plate) has been reported for a wide variety of materials. Further researches on the formation mechanism from nanoparticles might be necessary, because various phenomena are reported in literatures but their origins are not explained. For example, needlelike $PbTiO_3$ particles are formed by heating of a mixture of equiaxed $PbTiO_3$ particles, NaCl, and surfactant (Cai, et al., 2007) and non-equiaxed $BaTiO_3$ particles are prepared from equiaxed nano TiO_2 particles without a surfactant (Deng et al., 2009). Careful examination of product particles is necessary because the formation of titanium oxide-rich compounds, instead of $PbTiO_3$ and $BaTiO_3$, is possible (Rørvik et al., 2008).

6. Rererences

Afanasiev, P. & Geantet, C. (1998). Synthesis of Solid Materials in Molten Nitrates. *Coordination Chemistry Reviews*, Vol.178-180, Part 2, (December 1998), pp. 1725-1752, ISSN 0010-8545

Arendt, R. H., Rosolowski, J. H., & Szymaszek, J. W. (1979). Lead Zirconate Titanate Ceramics from Molten Salt Solvent Synthesized Powders. *Materials Research Bulletin*, Vol.14, No.5, (May 1979), pp. 703-709, ISSN 0025-5408

Arney, D., Porter, B., Greve, B., & Maggard, P. A. (2008). New Molten-Salt Synthesis and Photocatalytic Properties of $La_2Ti_2O_7$ Particles. *Journal of Photochemistry and Photobiology A: Chemistry*, Vol.199, No.2-3, (June 2008), pp. 230-235, ISSN 1010-6030

Cai, Z., Xing, X., Yu, R. Sun, X., & Liu, G. (2007). Morphology-Controlled Synthesis of Lead Titanate Powders. *Inorganic Chemistry*, Vol.46, No.18, (July 2007), pp. 7423-7427, ISSN 0020-1669

Deng, H., Qiu, Y., & Yang, S. (2009). General Surfactant-free Synthesis of $MTiO_3$ (M = Ba, Sr, Pb) Perovskite Nanostrips, *Journal Materials Chemistry*, Vol.19, No.7, (January 2009), pp. 976-982, ISSN 0959-9428

Elwell, D. & Scheel, H. J. (1975). *Crystal Growth from High-Temperature Solutions*, Academic Press, ISBN 0-12-237550-8, London, UK

Furubayashi, A. & Kimura, T. (2011). Preparation of Needlelike $Sr_{0.5}Ba_{0.5}Nb_2O_6$ Particles Using Molten $SrCl_2$-$BaCl_2$ Salt. *Journal of the Ceramic Society of Japan*, Vol.119, No.4 (April 2011), pp. 282-284, ISSN 0914-5400

Fuse, K. (2006). Mechanisms of Texture Development in $Bi_{0.5}(Na,K)_{0.5}TiO_3$ made by Reactive-Templated Grain Growth Method. *Master Thesis*, Keio University, Japan (March 2006)

Geselbracht, M. J., Walton, R. I., Cowell, E. S., Millange, F., & O'Hare, D. (2002). An Investigation of the Synthesis of the Layered Perovskite $RbCa_2Nb_3O_{10}$ Using Time-Resolved in Situ High-Temperature Powder X-ray Diffraction. *Chemistry of Materials*, Vol.14, Vol.10, (September 2002), pp. 4343-4349, ISNN 0897-4756

Han, C. -H., Hong, Y. -S., & Kim, K. (2003). Cyclic Performances of HT-$LiCo_{0.8}M_{0.2}O_2$ (M=Al, Ni) Powders Prepared by the Molten Salt Synthesis Method. *Solid State Ionics*, Vol.159, No.3-4, (April 2003), pp. 241-247, ISSN 0167-2738

Hayashi, Y., Kimura, T., & Yamaguchi, T. (1985). Mechanism of Flux-Aided Reaction in Ferrite Systems. *Bulletin of the American Ceramic Soc*iety, Vol.64, No.9, (September 1985), pp. 1249-52, ISSN 0002-7812

Hayashi, Y., Kimura, T., & Yamaguchi, T. (1986a). Preparation of Acicular NiZn-Ferrite Powders. *Journal of Materials Science*, Vol.21, No.8, (August 1986), pp. 2876-2880, ISSN 0022-2461

Hayashi, Y., Kimura, T., & Yamaguchi, T. (1986b). Preparation of Rod-Shaped $BaTiO_3$ Powder. *Journal of Materials Sci*ence, Vol.21, No.3, (March 1986), pp. 757-762, ISSN 0022-2461

Hillert, M. (1998). *Phase Equilibria, Phase Diagrams and Phase Transformations, Their Thermodynamic Basis*, Cambridge University Press, ISBN 0-521-56584-7, Cambridge, UK

Hofmeister, W., Tillmanns, E., & Baur, W. (1984). Refinement of Barium Titanate, $BaTi_4O_9$, and Hexabarium 17-Titanate, $Ba_6Ti_{17}O_{40}$. *Acta Crystallographica Section C*, Vol.40, No.9, (September 1984), pp. 1510-1512, ISSN 0108-2701

Huang, K. -C. Huang, T. -C., & Hsieh, W. -F. (2009). Morphology-Controlled Synthesis of Barium Titanate Nanostructures. *Inorganic Chemistry*, Vol.48, No.19, (September 2009) pp. 9180-9184 ISSN 0020-1669

Huang, Z., Li, B., & Liu, J. (2010). Molten-Salt Synthesis of Oxyapatite $La_{9.33}Si_6O_{26}$ Powders as Electrolytes for Intermediate Temperature Solid Oxide Fuel Cells. *Physica Status Solidi A – Application and Materials Science*, Vol.207, No.10, (August 2010), pp. 2247-2251, ISSN 1862-6300

Janz, G. J. (1967). *Molten Salt Handbook*, Academic press, LCCCN 66-30087, New York, USA

Jayaseelan, D. D., Zhang, S., Hashimoto, S., & Lee, W. E. (2007). Template Formation of Magnesium Aluminate ($MgAl_2O_4$) Spinel Microplatelets in Molten Salt. *Journal of the European Ceramic Society*, Vol.27, No.16, (June 2007), pp. 4745-4749, ISSN 0955-2219

Kang, S. -J. L., Lee, M. -G., & An, S. -M. (2009). Microstructure Evolution During Sintering with Control of the Interface Structure. *Journal of the American Ceramic Society*, Vol.92, No.7, (June 2009), pp. 1464-1471, ISSN 0002-7820

Kimura, T., Takahashi, T., & Yamaguchi, T. (1980). Preparation and Characteristics of Ni-Ferrite Powders obtained in the Presence of Fused Salts. *Journal of Materials Sci*ence, Vol.15, No.6, (June 1980), pp. 1491-1497, ISSN 0022-2461

Kimura, T., Takahashi, T., and Yamaguchi, T. (1981). Preparation of Ferrite Powder by Flux Method. *Ferrites, Proceedings of ICF 3,* pp. 27-29, UTP 3055-67543-5149, Kyoto, Japan September 29 – October 2, 1980

Kimura, T. & Yamaguchi, T. (1982). Morphology of Bi_2WO_6 Powders obtained in the Presence of Fused Salt. *Journal of Materials Sci*ence, Vol.17, No.7, (July 1982), pp. 1863-1870, ISSN 0022-2461

Kimura, T. & Yamaguchi, T. (1983). Fused Salt Synthesis of $Bi_4T_{i3}O_{12}$. *Ceramics International*, Vol.9, No.1, (January-March 1983), pp. 13-17 ISSN 0272-8842

Kimura, T., Yamaguchi, T., & Newnham, R. E. (1983a) Phase and Morphology of $PbNb_2O_6$ Obtained by Molten Salt Synthesis. *Particulate Science and Technology*, Vol.1, No.3, (July 1983), pp. 357-364 ISSN 0272-6351

Kimura, T., Machida, M., Yamaguchi, T., & Newnham, R. E. (1983b). Products of Reaction Between PbO and Nb_2O_5 in Molten KCl or NaCl. *Journal of the American Ceramic Society*, Vol.66, No.10, (October 1983), pp. C-195-C-197, ISSN 0002-7820

Kimura, T., Takenaka, A., Mifune, T., Hayashi, Y., & Yamaguchi, T. (1992). Preparation of Needle-like $TiZrO_4$ and PZT Powders. *Journal of Materials Science*, Vol.27, No.6, (June 1992), pp. 1479-1483, ISSN 0022-2461

Kimura, T., Miura, Y., & Fuse, K. (2005). Texture Development in Barium Titanate and PMN-PT using Hexabarium 17-Titanate Heterotemplates. *International Journal of Applied Ceramic Technology*, Vol.2, No.1, (January 2005), pp. 15-23, ISSN 1546-542X

Kimura, T. (2006). Application of Texture Engineering to Piezoelectric Ceramics – A Review. *Journal of the Ceramic Society of Japan*, Vol.114, No.1, (January 2006), pp. 15-25 ISSN 0914-5400

Kimura, T. & Yoshida, Y. (2006). Origin of Texture Development in Barium Bismuth Titanate Made by Templated Grain Growth Method. *Journal of the American Ceramic Society*, Vol.89, No.3, (January 2006), pp. 869-874, ISSN 0002-7820

Li, L., Deng, J., Chen, J., Sun, X., Yu, R., Liu, G., & Xing, X. (2009). Wire Structure and Morphology Transformation of Niobium Oxide and Niobates by Molten Salt Synthesis. *Chemistry of Materials*, Vol.21, No.7, (March 2009), pp. 1207-1213, ISNN 0897-4756

Liu, D., Yan, Y., & Zhou, H. (2007). Synthesis of Micron-Scale Platelet $BaTiO_3$. *Journal of the American Ceramic Society*, Vol.90, No.4, (March 2007), pp. 1323-1326, ISSN 0002-7820

Liu, Y. -F., Lu, Y. -N., Xu, M., Zhou, L. -F., & Shi, S. -Z. (2009). Topochemical Reaction of $SrTiO_3$ Platelet Crystals based on $Sr_3Ti_2O_7$ Platelet Precursor in Molten Salt Synthesis Process. *Materials Chemistry and Physics*, Vol.114, No.1, pp. 37-42, (November 2008), ISSN 0254-0584

Mao, Y., Banerjee, S., & Wong, S. S. (2003). Large-Scale Synthesis of Single-Crystalline Perovskite Nanostructures. *Journal of the American Chemical Society*, Vol.125, No.51 (November 2003), pp. 15718-15719, ISSN 0002-7863

Mao, Y., Park, T. -J., Zhang, F., Zhou, H., & Wong. S. S. (2007). Environmentally Friendly Methodologies of Nanostructure Synthesis. *Small*, Vol.3, No.7, (June 2007), pp. 1122-1139, ISSN 1613-6811

Messing, G. L., Trolier-McKinstry, S., Sabolsky, E. M., Duran, C., Kwon, S., Brahmaroutu, B., Park, P., Yilmaz, H., Rehrig, P. W., Eitel, K. B., Suvaci, E., Seabaugh, M., & Oh, K. S. (2004). Templated Grain Growth of Textured Piezoelectric Ceramics. *Critical Reviews in Solid State and Materials Science*, Vol.29, No.2, (June 2004), pp. 45-96, ISSN 1040-8436

Motohashi, T. & Kimura, T. (2008). Formation of Homo-Template Grains in $Bi_{0.5}Na_{0.5}TiO_3$ Prepared by Reactive-Templated Grain Growth Process. *Journal of the American Ceramic Society*, Vol.91, No.12, (November 2008), pp. 3889-3895, ISSN 0002-7820

Niesz, D. E. & Bennett, R. B. (1978). Structure and Properties of Agglomerates, In: *Ceramic Processing Before Firing*, G. Y. Onoda, Jr. & L. L. Hench, (Ed.), pp. 61-73, John Wiley & Sons, ISBN 0-471-65410-8, New York, USA

Park, J. -H., Lee, D. -H., Shin, H. -S., & Lee, B. -K. (1996). Transition of the Particle-Growth Mechanism with Temperature Variation in the Molted-Salt Method. *Journal of the American Ceramic Society,* Vol.79, No.4, (April 1996), pp. 1130-32, ISSN 0002-7820

Poterala, S. F., Chang, Y., Clark, T., Meyer, Jr, R. J., & Messing, G. L. (2010). Mechanistic Interpretation of the Aurivillius to Perovskite Topochemical Microcrystal Conversion Process. *Chemistry of Materials*, Vol.22, No.6, (February 2010), pp. 2061-2068, ISSN 0897-4756

Rahaman, M. N. (2003). *Ceramic Processing and Sintering* (2nd edition), Marcel Dekker, ISBN 0-8247-0988-8, New York, USA

Rørvik, P. M., Lyngdal, T., Sæterli, R., van Helvoort, A. T. J., Holmestad, R., Grande, T., & Einarsrud, M. -A. (2008). Influence of Volatile Chloride on the Molten Salt Synthesis of Ternary Oxide Nanorods and Nanoparticles. *Inorganic Chemistry*, Vol.47, No.8, (February 2008), pp. 3173-3181, ISSN 0020-1669

Saito, Y., Takao, H., Tani, T., Nonoyama, T., Takatori, K., Homma, T., Nagaya, T., & Nakamura, M. (2004). Lead-Free Piezoelectrics. *Nature*, Vol.432, No.7013, (October 2004), pp. 84-87, ISSN 0028-0836

Saito, Y. & Takao, H. (2006). Synthesis of Platelike {100} $SrTiO_3$ Particles by Topochemical Microcrystal Conversion and Fabrication of Grain-Oriented Ceramics. *Japanese Journal of Applied Physics*, Vol.45, No.9B, (September 2006), pp. 7377-7381, ISSN 0021-4922

Saito, Y. & Takao, H. (2007). Synthesis of Polycrystalline Platelike $KNbO_3$ Particles by the Topochemical Micro-Crystal Conversion Method and Fabrication of Grain-Oriented $(K_{0.5}Na_{0.5})NbO_3$ Ceramics. *Journal of the European Ceramic Society*, Vol.27, No.13-15, (April 2007), pp. 4085-4092, ISSN 0955-2219

Saito, Y., Takao, H., $ Wada, K. (2008). Synthesis of Platelike CaTiO3 Particles by a Topochemical Microcrystal Conversion Method and Fabrication of Textured Microwave Dielectric Ceramics. Ceramics International, Vol.34, No.4, (September 2007), pp. 745-751, ISSN 0272-8842

Sakurai, F. (2011). Mechanism of Texture Development in (K,Na)NbO_3-Based Ceramics. *Master Thesis*, Keio University, Japan (March 2011)

Sanson, A. & Whatmore, R. W. (2005). Phase Diagram of the $Bi_4Ti_3O_{12}$-$BaTiO_3$-$(Na_{1/2}Bi_{1/2})TiO_3$ System. *Journal of the American Ceramic Society*, Vol.88, No.11, (August 2005), pp. 3147-3135, ISSN 0002-7820

Santhanam, R. & Rambabu, B. (2010). Research Progress in High Voltage Spinel $LiNi_{0.5}Mn_{1.5}O_4$ Material. *Journal of Power Source*s, Vol.195, No.17, (March 2010), pp. 5442-5451 ISSN 0378-7753

Sato, T. & Kimura, T. (2008). Preparation of <111>-textured $BaTiO_3$ Ceramics by Templated Grain Growth Method Using Novel Template Particles. *Ceramics International*, Vol.34, No.4, (September 2007), pp. 757-760, ISSN 0272-8842

Schaak, R. E. & Mallouk, T. E. (2000). Topochemical Synthsesis of Three-Dimensional Perovskites from Lamellar Precursors. *Journal of the American Chemical Society*, Vol.122, No.12, (March 2000), pp. 2798-2803, ISSN 0002-7863

Schmalzried, H. (1995). *Chemical Kinetics of Solids*, VCH Verlagsgesellschaft mbH, ISBN 3-27-29094-X, Weinheim, Germany

Takahashi, T., Mogushi, N., Kimura, T., & Yamaguchi, T. (1981). Formation Mechanism of Ferrite Powders in Flux. *Bulletin of the Chemical Society of Japan*, Vol.1981, No.9, (September 1981), pp. 1391-1395, ISSN 0009-2673

Tani, T. & Kimura, T. (2006). Reactive-templated Grain Growth Processing for Lead-free Piezoelectric Ceramics. *Advances in Applied Ceramics*, Vol.105, No.1, (February 2006), pp. 55-63, ISSN 1743-6753

Tiano, A. L., Koenigsmann, C., Santulli, A. C., & Wong, S. S. (2010). Solution-based Synthetic Strategies for One-dimensional Metal-containing nanostructures. *Chemical Communications*, Vol.46, No.43, (September 2010), pp. 8093-8130, ISSN 1359-7345

Watari, K., Brahmaroutu, B., Messing, G. L., Trolier-McKinstry, S., & Cheng, S. -C. (2000). Epitaxial Growth of Anisotropically Shaped, Single-Crystal Particles of Cubic $SrTiO_3$. *Journal of Materials Research*, Vol.15, No.4, (April 2000), pp. 846-849, ISSN 0884-2914

Wickham, D. G. (1971). The Preparation of Ferrites with the Aid of Fused Salts. *Ferrites, Proceedings of the International Conference*, pp. 105-107, UTP 3055-67543-5149, Kyoto, Japan, July 6-9, 1970

Yan, B. & Lei, F. (2010). Molten Salt Synthesis, Characterization and Luminescence of $ZnWO_4$:Eu^{3+} Nanoparticles. *Journal of Alloys and Compounds*, Vol.507, No.2, (August 2010), pp. 460-464, ISSN 0925-8388

Yang, Z., Wei, L., Chang, Y., & Liu, B. (2007). Synthesis of Anisometric $KSr_2Nb_5O_{15}$ Particles in the $SrNb_2O_6$-Nb_2O_5-KCl System. *Journal of Materials Science*, Vol.42, No.10, (May 2007), pp. 3627-3631, ISSN 0022-2461

Yang, B., Yuan, X., & Chai, D. (2011). A Rational Self-Sacrificing Template Route to $LiMn_2O_4$ Nanotubes and Nanowires. *Journal of Nanomaterials*, Vol.2011, Article ID 197265, 5 pages, ISSN 1687-4129

Yoon, K. H., Cho, Y. S., & Kang, D. H. (1998). Molten Salt Synthesis of Lead-based Relaxors. *Journal of Materials Science*, Vol.33, No.12, (June 1998), pp. 2977-84, ISSN 0022-2461

Zhao, L., Gao, F., Zhang, C., Zhao, M., & Tian, C. (2005). Molten Salt Synthesis of Anisometric $KSr_2Nb_5O_{15}$ Particles. *Journal of Crystal Growth*, Vol.276, No.3-4, (December 2004), pp. 446-452, ISSN 0022-0248

Zhao, W., Zhou, H., Yan, Y., & Liu, D. (2008). Topochemical Synthesis of Plate-like $Na_{0.5}Bi_{0.5}TiO_3$ from Aurivillius Precursor. *Journal of the American Ceramic Society*, Vol.91, Vol.4, (January 2008), pp. 1322-1325, ISSN 0002-7820

Zhou, H., Mao, Y., & Wong, S. S. (2007). Probing Structure-Parameter Correlation in the Molten Salt Synthesis of $BaZrO_3$ Perovskite Submicrometer-Sized Particles. *Chemistry of Materials*, Vol.19, No.22, (October 2007), pp. 5238-5249, ISSN 0897-4756

Zeng, J. T., Kwok, K. W., Tam, W. K., Tian, H. Y., Jiang, X. P., & Chan, H. L. W. (2006). Plate-Like $Na_{0.5}Bi_{0.5}TiO_3$ Template Synthesized by a Topochemical Method. *Journal of the American Ceramic Society*, Vol.89, No.12, (October 2006), pp. 3850-3853, ISSN 0002-7820

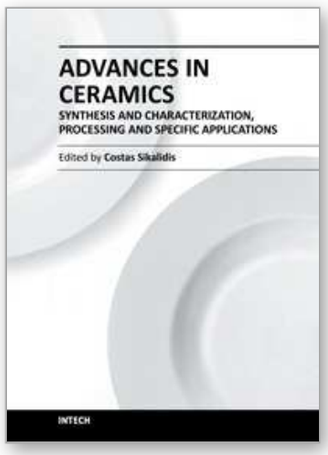

Advances in Ceramics - Synthesis and Characterization, Processing and Specific Applications

Edited by Prof. Costas Sikalidis

ISBN 978-953-307-505-1
Hard cover, 520 pages
Publisher InTech
Published online 09, August, 2011
Published in print edition August, 2011

The current book contains twenty-two chapters and is divided into three sections. Section I consists of nine chapters which discuss synthesis through innovative as well as modified conventional techniques of certain advanced ceramics (e.g. target materials, high strength porous ceramics, optical and thermo-luminescent ceramics, ceramic powders and fibers) and their characterization using a combination of well known and advanced techniques. Section II is also composed of nine chapters, which are dealing with the aqueous processing of nitride ceramics, the shape and size optimization of ceramic components through design methodologies and manufacturing technologies, the sinterability and properties of ZnNb oxide ceramics, the grinding optimization, the redox behaviour of ceria based and related materials, the alloy reinforcement by ceramic particles addition, the sintering study through dihedral surface angle using AFM and the surface modification and properties induced by a laser beam in pressings of ceramic powders. Section III includes four chapters which are dealing with the deposition of ceramic powders for oxide fuel cells preparation, the perovskite type ceramics for solid fuel cells, the ceramics for laser applications and fabrication and the characterization and modeling of protonic ceramics.

InTech Europe
University Campus STeP Ri
Slavka Krautzeka 83/A
51000 Rijeka, Croatia
Phone: +385 (51) 770 447
Fax: +385 (51) 686 166
www.intechopen.com

InTech China
Unit 405, Office Block, Hotel Equatorial Shanghai
No.65, Yan An Road (West), Shanghai, 200040, China
中国上海市延安西路65号上海国际贵都大饭店办公楼405单元
Phone: +86-21-62489820
Fax: +86-21-62489821

IntechOpen